

Electronic Supplementary Information

Evolution of Cu Single Atom Catalyst to Nanoclusters during CO₂

Reduction to CO

Liu Yan,^a Xiao-Du Liang,^a Yue Sun,^a Liang-Ping Xiao,^a Bang-An Lu,^b Guang Li,^a Yu-Yang Li,^a Yu-Hao Hong,^a Li-Yang Wan,^a Chi Chen,^c Jian Yang,^{*a} Zhi-You Zhou,^a Na Tian^{*a} and Shi-Gang Sun^a

^a State Key Laboratory of Physical Chemistry of Solid Surfaces, Collaborative Innovation Center of Chemistry for Energy Materials, College of Chemistry and Chemical Engineering, Xiamen University, Xiamen 361005, China. E-mail: tnsd@xmu.edu.cn; wjianyang@xmu.edu.cn

^b School of Material Science & Engineering, Zhengzhou University, Zhengzhou 450001, China.

^c Shanghai Advanced Research Institute, Chinese Academy of Sciences, Shanghai 201210, China

Experimental details

Chemicals

Zinc nitrate hexahydrate (Zn(NO₃)₂·6H₂O, 99%), copper acetate monohydrate (Cu(CH₃COO)₂·H₂O, 99%), Methanol (CH₃OH, >99.5%), n-hexane and N, N-2 methylformamide were all obtained from Sinopharm Chemical Reagent Co. Ltd. Potassium bicarbonate (KHCO₃), 2-methylimidazole (99%) and dicyandiamide were purchased from Aladdin Industrial Corporation. All chemicals were of analytical grade and used without further treatment. The ultrapure water (18.2 MΩ cm) used in all experiments was generated by Mili-Q Nanopure water system.

Material Characterization

SEM images were measured on Hitachi S4800 operated at 15 kV. TEM, HR-TEM measurements were performed on TECNAI F20 at an acceleration voltage of 200 kV. STEM and elemental mapping were taken on FEI Talos F200s at an acceleration voltage of 200 kV. HAADF-STEM was carried out on FEI Themis Z instrument operated at 200 kV with cold field-emission gun and aberration corrector, and the samples were prepared by dropping ethanol dispersion of samples onto copper microgrid. XRD patterns were taken on a Rigaku Ultima IV diffractometer (Rigaku, Japan) with Cu Kα X-ray source. XPS measurements were conducted on Escalab 250xi (Thermo Fisher Scientific, America) using Al Kα radiation (1486.6 eV) as the X-ray source. Binding energies reported herein are with reference to C (1s) at 284.5 eV. The concentration of Cu element in samples were determined by the ICP-MS (Agilent 720ES).

Synthesis

Synthesis of CuZIF-8: According to previous reports¹⁻³, Cu doped ZIF-8 was synthesized by hydrothermal method. First, 0.064 mol 2-methylimidazole and 0.0016 mol $\text{Cu}(\text{CH}_3\text{COO})_2 \cdot \text{H}_2\text{O}$ were dissolved in 120 mL anhydrous methanol (solution A), and 0.016 mol $\text{Zn}(\text{NO}_3)_2 \cdot 6\text{H}_2\text{O}$ were dissolved in 80 mL anhydrous methanol (solution B). After ultrasonic treatment for 10 min, the solution B was poured into solution A, and pre-stirred for 30 min at room temperature, then the mixture was transferred into Teflon-lined autoclave and heated at 120 °C for 4 h. After being cooled to room temperature, the products were washed with methanol several times. The CuZIF-8 was obtained after being dried at 60 °C under vacuum overnight. The synthesis of ZIF-8 was similar except removing the Cu^{2+} precursor.

Synthesis of CuZIF-8-DCD: 200 mg of as-synthesized CuZIF-8 and 200 mg of dicyandiamide were added into 50 mL of n-hexane and 1 mL DMF, respectively. The above DMF solution of the dicyandiamide was added into the n-hexane solution of CuZIF-8 bit by bit. After ultrasound for 2 h, the supernatant was carefully poured out after standing to distinct layering, and the bottom precipitation was put into the vacuum drying oven at 50 °C overnight to obtain CuZIF-8-DCD.

Synthesis of CuNC-DCD: The precursors CuZIF-8-DCD was placed in a tube furnace. The temperature was kept at 350 °C for 1 h under N_2 atmosphere, and then increased to 1000 °C for 4 h for pyrolysis. The heating rate was set to 5 °C/s. After cooled gradually to room temperature, the black powder were obtained and designated as CuNC-DCD. The synthesis of NC was similar except changing the precursor CuZIF-8-DCD into ZIF-8.

Electrochemical measurement

Preparation of working electrode: The working electrode was prepared as follow. A catalyst ink was prepared by dispersing the catalysts into an Nafion solution (1 mL comprised of 0.4 mL isopropyl alcohol, 0.6 mL ultra-pure water and 30 μL 5 wt% Nafion), and then sonicated for more than 30 min to be homogeneous. The obtained catalyst ink was uniformly dropped cast onto the untreated carbon cloth ($0.5 \text{ cm}^2 \times 2$) with a catalyst loading of $0.6 \text{ mg} \cdot \text{cm}^{-2}$, followed by drying carefully under infrared lamp before use.

The preparation of the working electrode in the ATR-IR experiment was as follows. 2 mg catalyst was placed in the sealed bottle, then 1 mL Nafion solution (0.4 mL isopropyl alcohol, 0.6 mL ultrapure water and 10 μL 5 wt % Nafion) was added, the catalyst ink was evenly mixed by ultrasonic. 30 μL catalyst ink

was absorbed and uniformly coated on the surface of the gold-plated monocrystalline silicon prism by drops, and then dried naturally.

Electrochemical measurements: All the experiments were carried out on a CHI760D electrochemical workstation with a three-electrode system at room temperature. A commercial gas-tight H-type cell was used with the cathode chamber and anode chamber separated by a proton exchange membrane (Nafion 117), and the electrolyte was 0.5 M KHCO₃ solution. The working electrode was prepared carbon cloth, the reference electrode was saturated calomel electrode (SCE), and the counter electrode was graphite sheet (2 × 3 cm²). Prior to electroreduction of CO₂, the cathodic electrolyte was bubbled with CO₂ (99.99%, Xinhang Fuzhou Inc.) for at least 30 min to ensure that CO₂ was dissolved to saturation in the electrolyte. All potentials were converted to RHE reference scale by the equation, $E_{\text{RHE}} = E_{\text{SCE}} + 0.241 + 0.0591 \times \text{pH}$. The pH values of CO₂-saturated 0.5 M KHCO₃ was 7.2. The current densities in this work were all normalized to the geometric surface area. CO₂RR measurements were conducted with CO₂ continuously purged into the cathodic compartment and kept at 10 mL·min⁻¹, with the catholyte magnetically stirred during the electrolysis. The Faradaic efficiency of each gas products were calculated by the equation:

$$FE = \frac{2 \times 96500(C \cdot \text{mol}^{-1}) \times V(\text{mL} \cdot \text{min}^{-1}) \times 10^{-6}(\text{m}^3 \cdot \text{mL}^{-1}) \times v(\text{vol}\%) \times 1.013 \times 10^5(\text{N} \cdot \text{m}^{-2})}{8.314(\text{N} \cdot \text{m} \cdot \text{mol}^{-1} \cdot \text{K}^{-1}) \times 298.15(\text{K}) \times j_{\text{Total}}(\text{C} \cdot \text{s}^{-1}) \times 60(\text{s} \cdot \text{min}^{-1})}$$

where v (vol %) is volume concentration of CO in the exhaust gas from the cell (gas chromatography data), V (mL·min⁻¹) is gas flow rate measured by a flow meter at the exit of the cell at room temperature and under ambient pressure, and j_{Total} (C·s⁻¹) is steady-state current⁴.

Analytical method

The gas products of CO₂ electroreduction from the cathode compartment were analyzed using an on-line gas chromatography (GC, Fuli9070) equipped with a flame ionization detector (FID, column: Porapak Q) and a thermal conductivity detector (TCD, column: 5A molecular sieve). The FID with methanizer was used to quantify CO, CH₄, C₂H₄, and C₂H₆, and the TCD was used to quantify H₂. The liquid phase products were quantitatively analyzed by ¹HNMR (Bruker AVANCEAV III HD 500). 500 μL of the reaction solution was prepared by adding 100 μL deuterium water (D₂O lock field) and 0.01 μL dimethyl sulfoxide (DMSO as internal standard) for test. The solvent pre-saturation method was used for the water peak suppression.

The diameter of Cu is about 0.25 nm according to the lattice constant of Cu (0.3608nm). As for analysis of atomic-resolved HAADF-STEM images, the bright spots with the size about 0.25 nm in were attributed to Cu single atoms, and those larger than 0.6 nm were assigned to nanoclusters.

Computational

All spin-polarized computations were carried out with the Vienna Ab initio Simulation Package. The PBE functional in combination with the Van der Waals correction was applied in this study^{5, 6}. The kinetic cut-off energy was 400 eV. The Brillouin zone was sampled with a 5×5×1 k-point mesh of the Monkhorst–Pack scheme. The vacuum layer between the periodic images of carbon layer was 20 Å. During the geometry optimization, all atoms were allowed to relax in the supercell, and the dipole correction was included. The energy convergence criterion was 10⁻⁵ eV, and the final forces were less than 0.01 eV Å⁻¹ at each atom. The computational hydrogen electrode model was applied to calculate the reaction free energy involving the electron-proton transfer⁷. The H₂ entropy in the gas phase was taken from the experimental value. The Cu(100) surface was simulated by a five-layer slab, in which the two bottom layers were fixed and the Cu lattice constant was 3.571 Å. The free energy correction at room temperature was carried out by the numerical frequency computation.

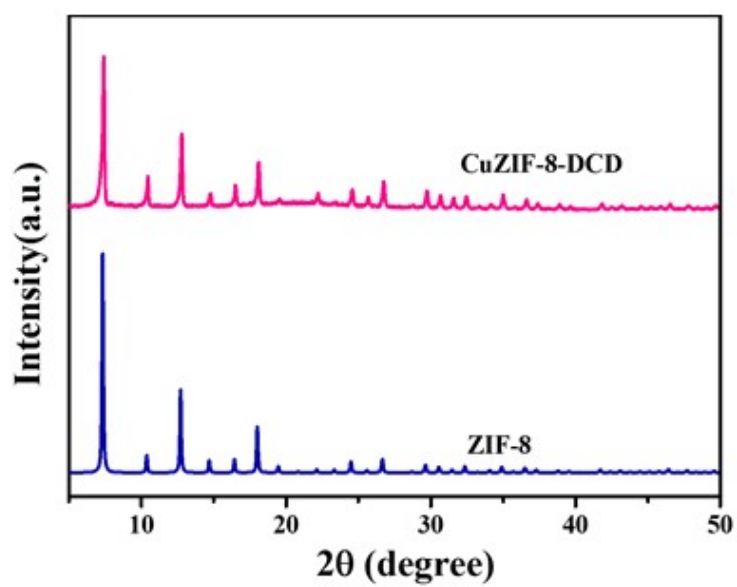


Fig. S1. XRD patterns of ZIF-8 and CuZIF-8-DCD.

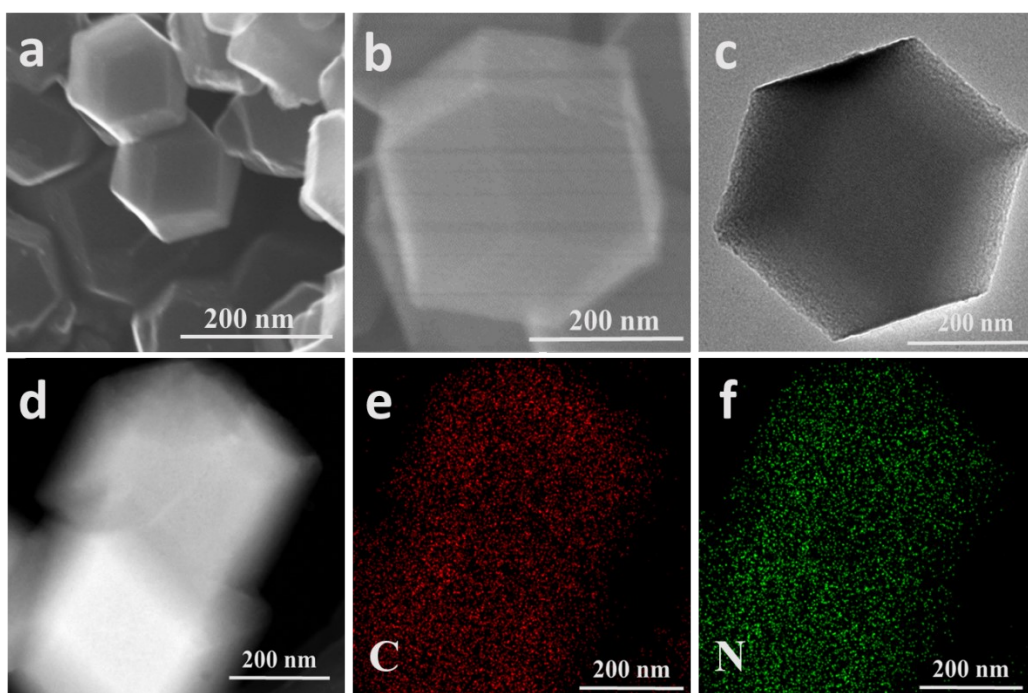


Fig. S2. Characterizations of NC sample. a)-b) SEM. c) TEM. d)-f) HADDF-STEM and corresponding EDS elemental mappings.

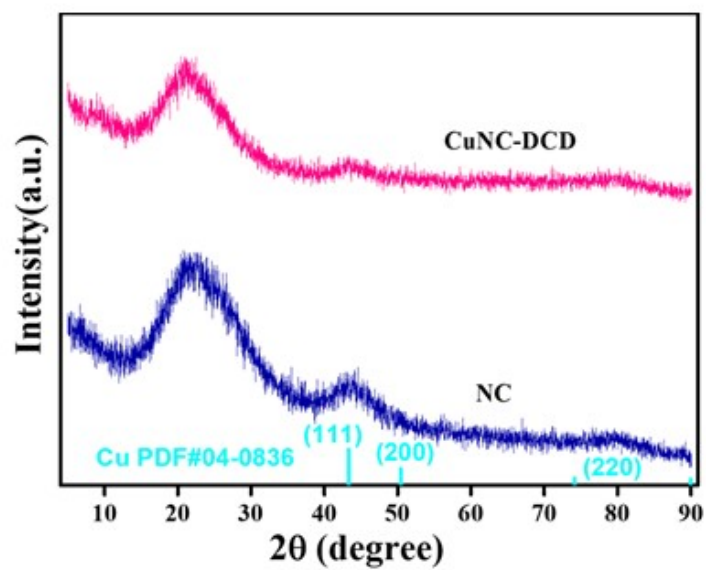


Fig. S3. XRD of CuNC-DCD and NC.

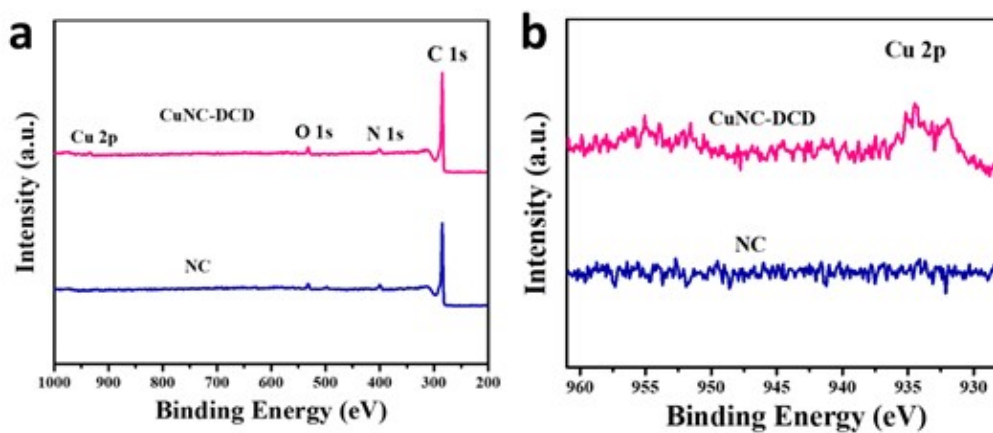


Fig. S4. a) Survey XPS and b) high-resolved Cu 2p spectra of CuNC-DCD and NC.

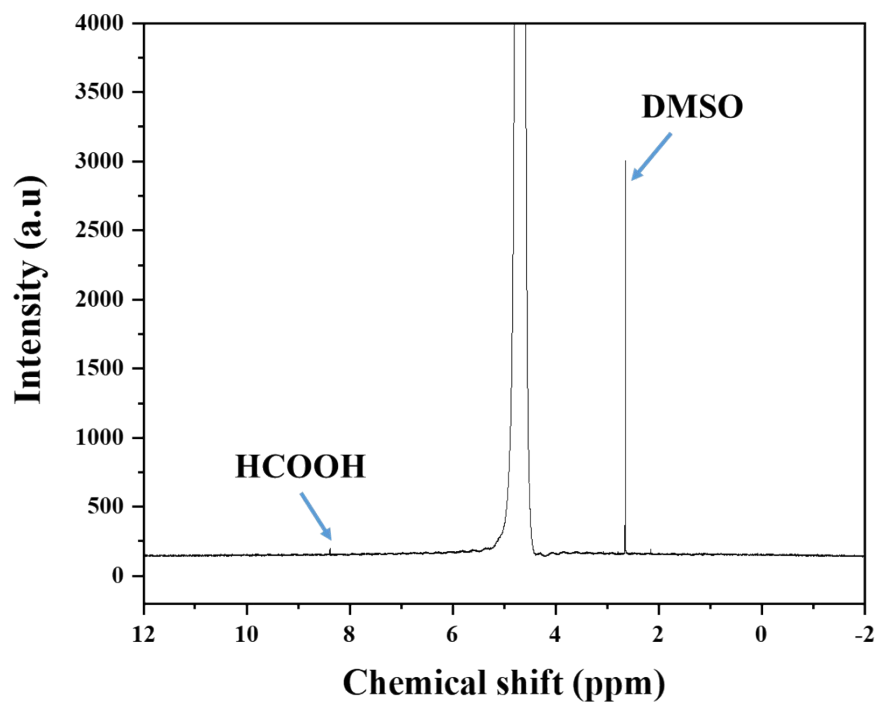


Fig. S5. ^1H NMR spectrum of liquid products for CO₂RR on CuNC-DCD at -0.50 V (vs RHE).

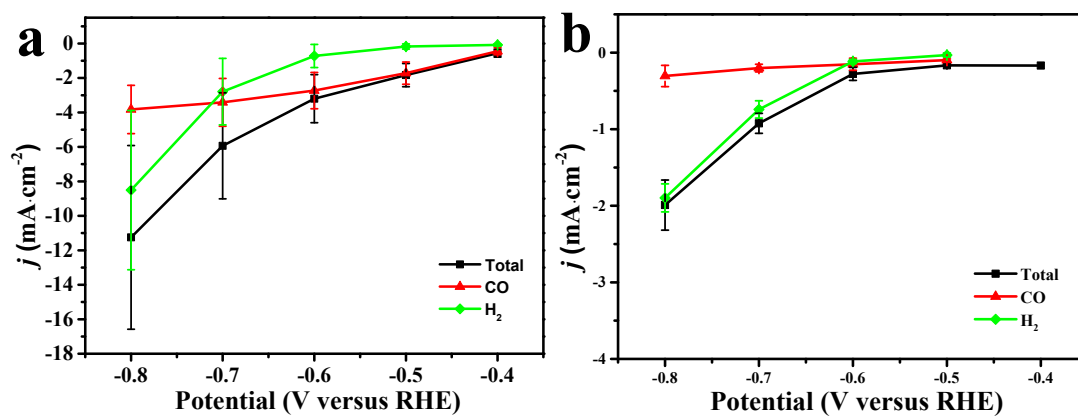


Fig. S6. Comparison of CO₂ electroreduction current density with error bar between a) CuNC-DCD and b) NC.

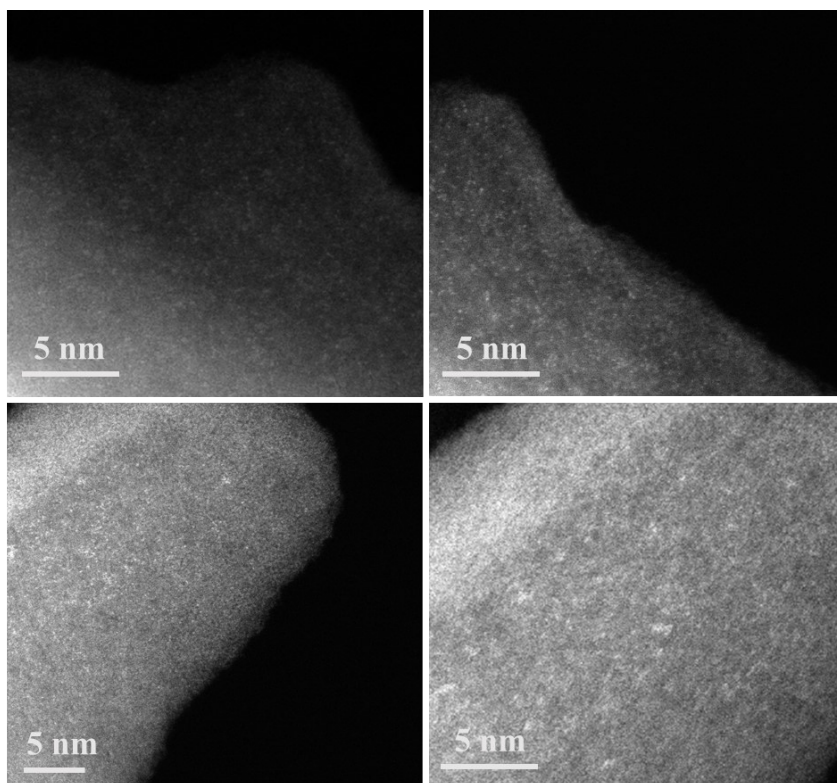


Fig. S7. HAADF-STEM images of CuNC-DCD after CO₂RR test at -0.20 V (vs RHE) for 30 min.

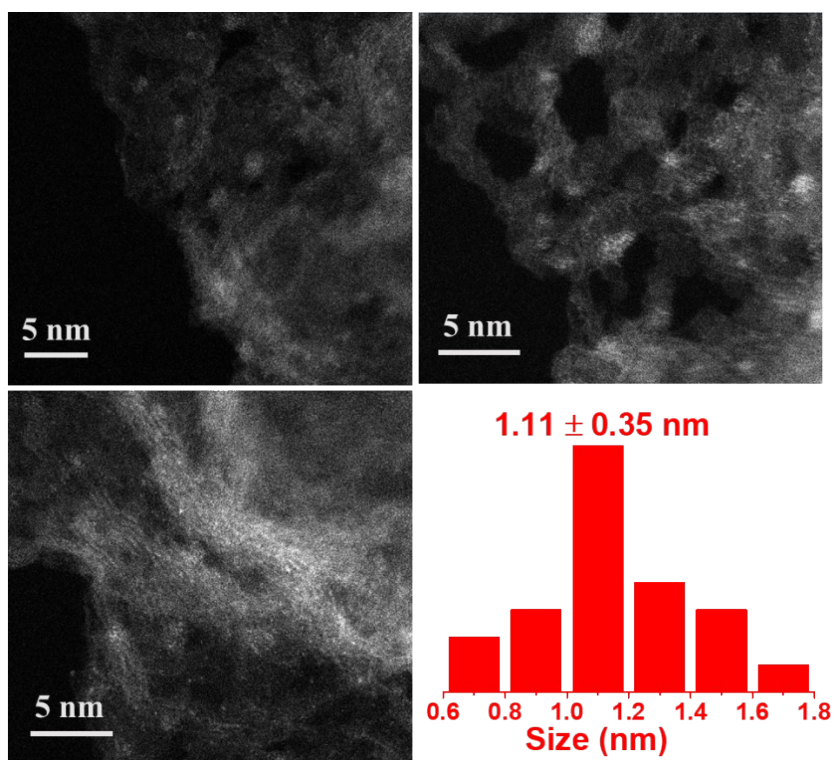


Fig. S8. HAADF-STEM images and particle size histogram of CuNC-DCD after CO₂RR test at -0.30 V (vs RHE) for 30 min.

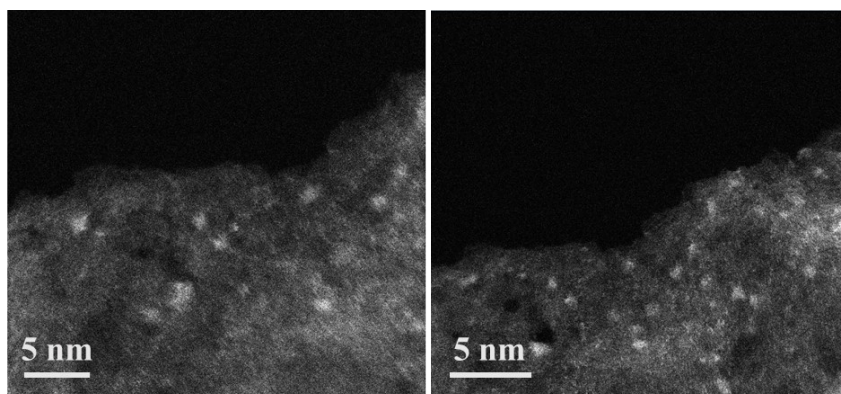


Fig. S9. HAADF-STEM images and particle size histogram of CuNC-DCD after CO₂RR test at -0.50 V (vs RHE) for 30 min.

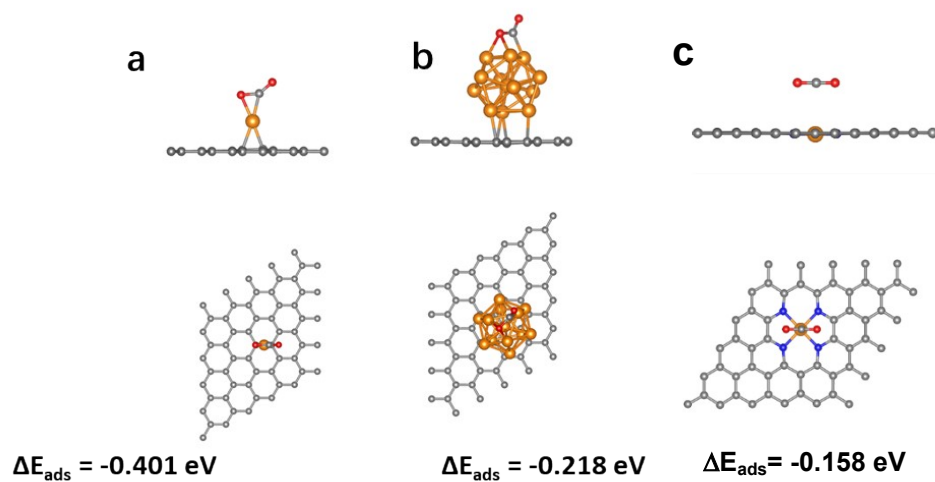


Fig. S10. *CO₂ adsorption configurations of the Cu center of **a)** Cu₁ and **b)** Cu₁₃ on the graphitic layer, c) CuN₄ site.

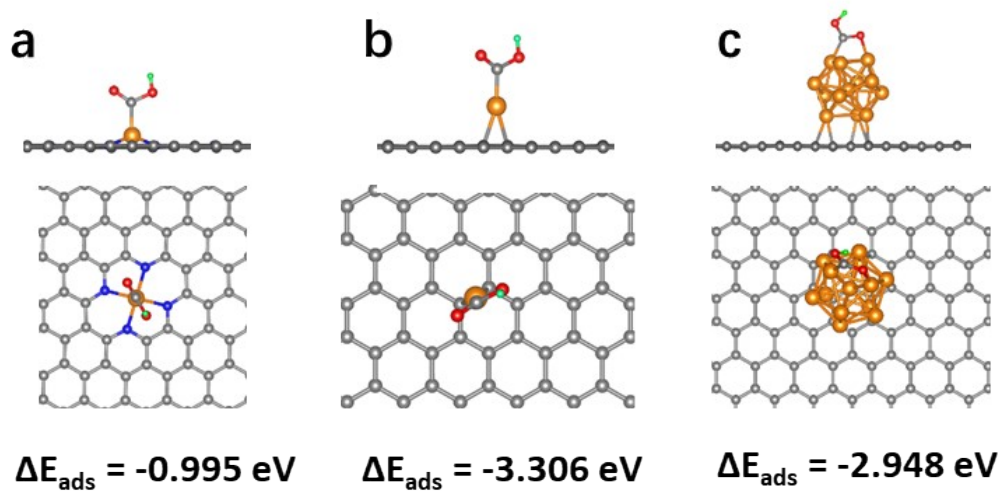


Fig. S11. *COOH adsorption configurations of the Cu center of **a)** CuN₄ in the graphitic layer, **b)** Cu₁ and **c)** Cu₁₃ on the graphitic layer.

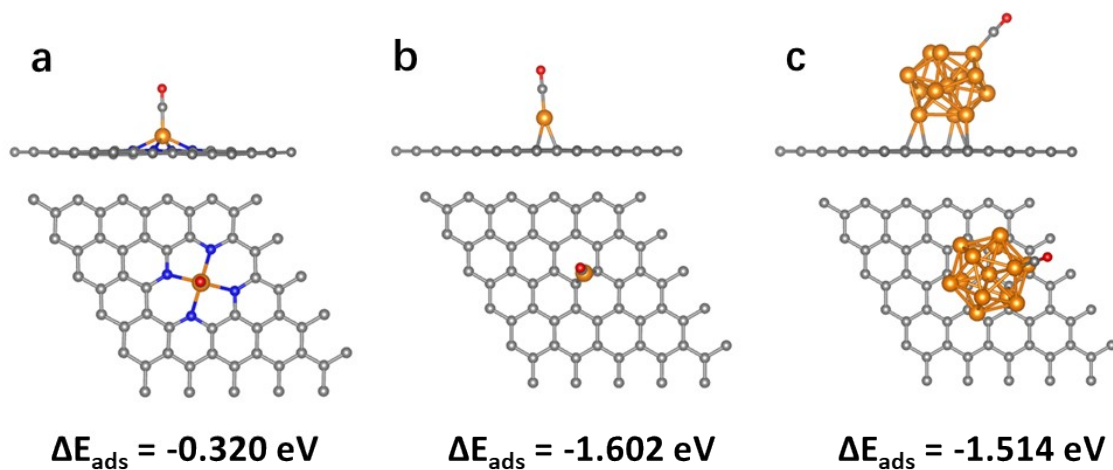


Fig. S12. *CO adsorption configurations of the Cu center of **a)** CuN₄ in the graphitic layer, **b)** Cu₁ and **c)** Cu₁₃ on the graphitic layer.

Table S1. Atomic mass fraction of Cu, Zn in NC and CuNC-DCD by inductively coupled plasma optical emission spectrometry (ICP-OES).

sample	Cu(wt.%)	Zn(wt.%)
NC	—	2.71
CuNC-DCD	1.12	1.22

Table S2. Comparison of CO₂RR performance between CuNC-DCD and NC at different potentials.

Sample	E (V vs RHE)	j_{total} (mA·cm ⁻²)	FE _{CO} (%)	FE _{H₂} (%)	j_{CO} (mA·cm ⁻²)	j_{H_2} (mA·cm ⁻²)
NC	-0.4	0.169	/	/	/	/
	-0.5	0.167	58.6	19.5	0.098	0.032
	-0.6	0.278	52.4	42.7	0.151	0.115
	-0.7	0.924	22.6	80.2	0.202	0.742
	-0.8	1.99	16.3	96.1	0.305	1.90
CuNC-DCD	-0.4	0.559	78.2	12.8	0.446	0.082
	-0.5	1.83	93.5	8.8	1.72	0.171
	-0.6	3.20	86.4	20.9	2.73	0.721
	-0.7	5.94	59.6	46.8	3.42	2.79
	-0.8	11.25	35.3	76.1	3.83	8.51

Table S3. Energies (E_{ads} and G_{ads}) related to CO_2 adsorption and $\angle\text{O-C-O}$ angle and the C-O bond length for the single-Cu atom and the Cu nanoclusters on the carbon layer, CuN_4 in the graphitic layer and Cu(100) (the C-O bond length in CO_2 molecule is computed to be 1.177 Å in gas phase).

	$E_{\text{ads}} / \text{eV}$	$G_{\text{ads}} / \text{eV}$	$\angle\text{O-C-O}$	C-O / Å
$\text{Cu}_1\text{-C}$	-0.401	-0.364	144.253	1.271, 1.203
$\text{Cu}_{13}\text{-C}$	-0.218	-0.176	126.952	1.337, 1.220
Cu(100)	0.147	0.172	128.294	1.324, 1.219
CuN_4	-0.158	-0.074	179.406	1.177, 1.177

It was found that there was a very weak molecular interaction between CO_2 and the CuN_4 site. However, the distance between the Cu center and the C atom of CO_2 molecule is ca. 3.217 Å, which cannot be considered for a Cu-C chemical bond as shown in the $\text{Cu}_1\text{-C}$, $\text{Cu}_{13}\text{-C}$ and Cu(100) structures. The $\angle\text{O-C-O}$ bond angle and C-O bond length related to the CuN_4 structure are identical to those of CO_2 molecule in gas phase (Table S3), indicating negligible activation of CO_2 molecule by the CuN_4 . This feature was remained when the cut-off energy was increased to 500 eV. The free energy of CO_2 adsorption on the CuN_4 site was ca. -0.074 eV, which was almost equal to the energy level of CO_2 molecule in the free energy profile. It implied that the spontaneous adsorption of CO_2 molecule at the Cu center could not be favored considerably at the CuN_4 structure. The spontaneous CO_2 adsorption could occur at the $\text{Cu}_1\text{-C}$ and $\text{Cu}_{13}\text{-C}$ structures; consequently, CO_2 can be activated to some extent.

References

1. K. Zhao, X. Nie, H. Wang, S. Chen, X. Quan, H. Yu, W. Choi, G. Zhang, B. Kim and J. G. Chen, *Nat Commun*, 2020, **11**, 2455.
2. X. Chen, N. Wang, K. Shen, Y. Xie, Y. Tan and Y. Li, *ACS Appl. Mater. Interfaces*, 2019, **11**, 25976-25985.
3. Y. Chen, S. Ji, Y. Wang, J. Dong, W. Chen, Z. Li, R. Shen, L. Zheng, Z. Zhuang, D. Wang and Y. Li, *Angew. Chem. Int. Ed.*, 2017, **56**, 6937-6941.
4. J. Jiao, R. Lin, S. Liu, W.-C. Cheong, C. Zhang, Z. Chen, Y. Pan, J. Tang, K. Wu, S.-F. Hung, H. M. Chen, L. Zheng, Q. Lu, X. Yang, B. Xu, H. Xiao, J. Li, D. Wang, Q. Peng, C. Chen and Y. Li, *Nat. Chem.*, 2019, **11**, 222-228.
5. S. Grimme, S. Ehrlich and L. Goerigk, *J. comput. chem.*, 2011, **32**, 1456-1465.

6. J. P. Perdew, K. Burke and M. Ernzerhof, *Phys. Rev. Lett.*, 1996, **77**, 3865-3868.
7. A. A. Peterson, F. Abild-Pedersen, F. Studt, J. Rossmeisl and J. K. Nørskov, *Energy Environ. Sci.*, 2010, **3**, 1311-1315.